

Study of effect of a smooth hump on hypersonic boundary layer stability by using PSE

*Donghun Park¹⁾ and Seung O Park²⁾

¹⁾ *Aerodynamics Research Team, KARI, Daejeon 305-806, Korea*

²⁾ *Department of Aerospace Engineering, KAIST, Daejeon 305-701, Korea*

¹⁾ kpdh84@kari.re.kr

²⁾ sopark@kaist.ac.kr

ABSTRACT

Effect of a two-dimensional smooth hump on linear instability of hypersonic boundary layer is studied by using parabolized stability equations (PSE). Linear evolution of mode S over a hump in Mach 4.5 and 5.92 flat plate boundary layers is analyzed. Mean flow for stability analysis is obtained by solving the parabolized Navier-Stokes (PNS) equations. Hump with height smaller than local boundary layer thickness is used. As same with the previous observations, destabilization effect on flat plate boundary layer is confirmed for hump located at upstream of synchronization point. On the other hand, stabilization effect is observed for hump at downstream of synchronization point. Parametric studies are carried to examine the effect of hump height, location, etc. Stabilization influence of hump on convective instability of mode S is found to be a possible cause of previous experimental observations of delaying transition in hypersonic boundary layers

1. INTRODUCTION

Roughness elements significantly affect boundary layer stability and transition and thus understanding and evaluation of the effect of roughness element on boundary layer instability is practically important. Many experimental studies observed the upstream shift of transition location due to roughness. Theoretical studies confirmed that two-dimensional smooth roughness destabilize convective instability. Recent numerical studies revealed that depending on the shape and size of the roughness, many instability mechanisms other than the normal mode instability can be involved in transition process. Most of previous studies have found that roughness element destabilize boundary layer leading to earlier transition.

On the other hand, for hypersonic flows, several experimental studies observed that roughness element can delay transition under certain circumstances. Holloway and

¹⁾ Senior Researcher

²⁾ Professor

Sterrett (1964) carried out experiments on flat plate boundary layer of Mach number of 4.0 and 6.0 with roughness. They observed delay of transition by the roughness with height smaller than local boundary layer thickness at a specific configuration. Fujii (2006) performed experiments on sharp cone boundary layer of Mach number of 7.1 with two-dimensional roughness. They also observed delaying of transition at certain conditions. These observations imply that roughness has a possibility to stabilize hypersonic boundary layer. The cause and underlying mechanism of this transition delay, however, were not disclosed in their studies.

Most dominant instability wave which leads hypersonic boundary layer transition is known to be Mack's 2nd mode. This mode is recently termed as mode 'S' by Fedorov and Tumin (2011). It is natural that influence of roughness on the convective instability of mode S need to be examined first to investigate the cause of delaying transition. Duan et al. (2009, 2010) and Fong et al. (2011) investigated roughness effect on instability of mode S by using direct numerical simulations (DNS). Their DNS studies showed that the roughness located at the downstream of synchronization point can stabilize mode S. Although they imposed mode S at the inflow boundary and focused on its downstream evolution, it is possible in DNS study that the other mechanisms other than the convective instability of mode S can be involved due to roughness. In this respect, study on the effect of roughness on convective instability can be important to make it clear that the transition delay is indeed associated with the stabilization of mode S.

In this study, theoretical study on the effect of a two-dimensional roughness on convective instability of mode S in hypersonic boundary layers is carried out by using parabolized stability equations (PSE). Flat plate boundary layer at two different Mach numbers. Smooth hump with height smaller than local boundary layer thickness is used as roughness geometry. Mean flow for stability analysis is obtained by solving the parabolized Navier-Stokes (PNS) equations. Spatial linear stability analysis is carried out to identify synchronization point. Linear evolution of mode S is studied for hump located at both upstream and downstream of the synchronization point. Parametric studies are performed to evaluate the effect of hump location and height. Overall influence of hump is examined by using *N*-factor curves for various frequencies.

2. METHOD OF ANALYSIS

2.1 Hump Geometry

Figure 1 shows schematically the two-dimensional smooth hump used in the present study. L , b and h represent respectively the distance from the leading edge of flat plate to the location of the hump center, half width, and height of the hump. The Reynolds number Re_L is defined as $U_\infty L/\nu$ where U_∞ is the free-stream velocity. The geometry of the hump is given by Eq. (1), which is the same with that used in previous studies (Nayfeh 1988 and Masad 1994)

$$y = h f(t) \quad (1)$$

where

$$t = (x - L) / b ; \quad f(t) = \begin{cases} 1 - 3t^2 + 2|t|^3 & , \text{if } |t| \leq 1 \\ 0 & , \text{if } |t| > 1 \end{cases}$$

$Re_L = U_\infty L / \nu$: Reynolds Number

L : distance from leading edge to center of hump

b : hump half width

h : hump height

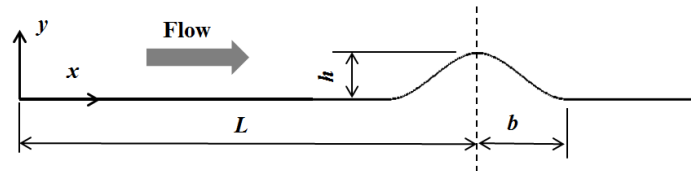


Fig. 1 Schematic of hump geometry

2.2 Parabolized Navier-Stokes Equations

The mean flow data of supersonic/hypersonic boundary layer over a hump are obtained by solving parabolized Navier-Stokes (PNS) equations. Formulation and solution techniques of PNS can be found in many references (Tannehill et al. 1999, 2000). The accuracy of PNS solution as basic flow for linear stability analysis of axisymmetric flows was verified by Esfahanian and Hejranfar (2007). In this study, the time iterative PNS (TIPNS) scheme of Tannehill et al. (1999, 2000) is employed. A computer code for PNS solution for both 2-D and axisymmetric flows with iterative procedure was made and was validated through several typical axisymmetric flow cases. This code was used to get mean flow data for the present stability analysis.

2.3 Parabolized Stability Equations

As is well known, PSE can take into account the flow non-parallelism and curvature effect on the stability analysis. The PSE approach is computationally more efficient than LST since it performs the stability analysis by downstream marching from the initial condition without solving eigenvalue problem at each streamwise station. Further, it also enables us to carry out non-linear stability study. The PSE has widely been used to study linear and non-linear stability of subsonic and supersonic boundary layers over simple geometries. The PSE formulation and solution technique can be found in many references (Herbert 1997, Chang et al. 1993, Chang 2004). The PSE method of the present study is the same with that of our previous work for incompressible and supersonic boundary layers (Park and Park 2013). Descriptions of the PSE formulation of the present study here can be found in them.

3. SPATIAL LINEAR STABILITY ANALYSIS AND SYNCHRONIZATION POINT

3.1 Spatial Linear Stability Analysis

To examine the effect of hump location with respect to synchronization point, the synchronization point of flat plate without hump is identified first by using spatial linear stability analysis. Flat plate boundary layer of Mach 4.5 with free-stream temperature of 61.11 K is considered following the case of Fedorov and Tumin (2011). Free-stream unit Reynolds number is set to 10^7 /m based on ideal gas relation ($p_\infty = 1008.64$ Pa). Similarity solution of compressible boundary layer with adiabatic wall condition is used

as mean flow and parallel flow approximation is employed. The similarity solution was obtained from the boundary layer code which is 4th order accurate in surface normal direction as described in Iyer (1990). Spatial linear stability analysis is carried out for $F=50$ at various streamwise locations. The non-dimensional frequency F is defined

$$F = \frac{2\pi f v_\infty}{(U_\infty)^2} \times 10^6 \quad (2)$$

Since the spatial stability is concerned, the nonlinear term of α appear in the eigenvalue problem. Non-linear terms are preserved and non-linear eigenvalue problem is reduced to linear eigenvalue problem as given in Malik (1990). Discretization with fourth order finite difference approximation yields matrix eigenvalue problem for α . The boundary layer length scale δ and Reynolds number based on this length scale (denoted as R) is widely used in the stability study to represent streamwise location.

$$\delta = \frac{x}{\sqrt{Re_x}} = \sqrt{\frac{\mu_\infty x}{\rho_\infty U_\infty}}; \quad R = \frac{\rho_\infty U_\infty \delta}{\mu_\infty} = \sqrt{\frac{\rho_\infty U_\infty x}{\mu_\infty}} = \sqrt{Re_x} \quad (3)$$

Figure 2 shows the eigenvalue spectra for $F=50$ at $R=2000$ ($x=0.4$ m). Abscissa and ordinate represent real and imaginary part of the eigenvalue, respectively. Vertically aligned eigenvalues in the figure correspond to entropy and vorticity mode spectrum. Horizontally distributed eigenvalues are spectra of fast (left hand side) and slow (right hand side) acoustic mode. Two discrete modes, mode S and mode F are originated from the slow and fast acoustic spectrum. It is well-known that mode S and mode F are named after the observation that they synchronizes with slow and fast acoustic wave near the leading edge. As highlighted in the figure, mode S and mode F are located at around the end of the slow and fast acoustic spectrum, respectively.

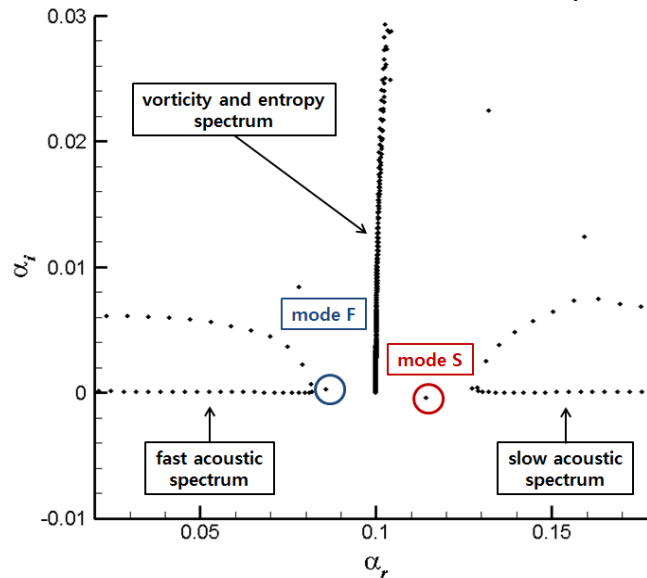


Fig. 2 Eigenvalue spectra from spatial stability analysis

3.2 Synchronization Point

Figure 3a shows the real part of phase speed of mode F and mode S with respect to R . The phase speed is obtained by $c = \omega/\alpha$. Present results are plotted with symbols and those of Fedorov and Tumin (2011) are plotted in dashed line in the figure. Figure 3a clearly shows that both results are in good agreement with each other. As described in Fedorov and Tumin in detail, mode F and mode S synchronize with fast and slow acoustic wave near the leading edge (low R), respectively. The phase speed of fast and slow acoustic wave are $1+M_\infty^{-1}=1.222$ and $1-M_\infty^{-1}=0.778$ which are indicated as horizontal solid lines in the figure. As R increases, phase speed of mode F decreases and synchronizes with that of vorticity and entropy mode ($c_r=1$) at around $R \approx 3316$. There is jump of phase speed of mode F when it crosses the vorticity and entropy spectrum as theoretically shown by Fedorov and Khokhlov (2001). Further downstream, phase speed of mode F decreases and synchronizes with mode S at around $R \approx 3808$. As seen in the figure, the phase speed of mode S increases continuously until it synchronizes with mode F. The location at which phase speeds of mode S and mode F synchronize is called as synchronization point. For the case given in the figure, the synchronization point ($R_s=3808$) corresponds to streamwise location of $x \approx 1.45$ m. Beyond the synchronization point, phase speed of mode F decreases continuously even lower than that of mode S. Imaginary part of phase speed plotted in Fig. 3b also shows good agreement with those given by Fedorov and Tumin (2011).

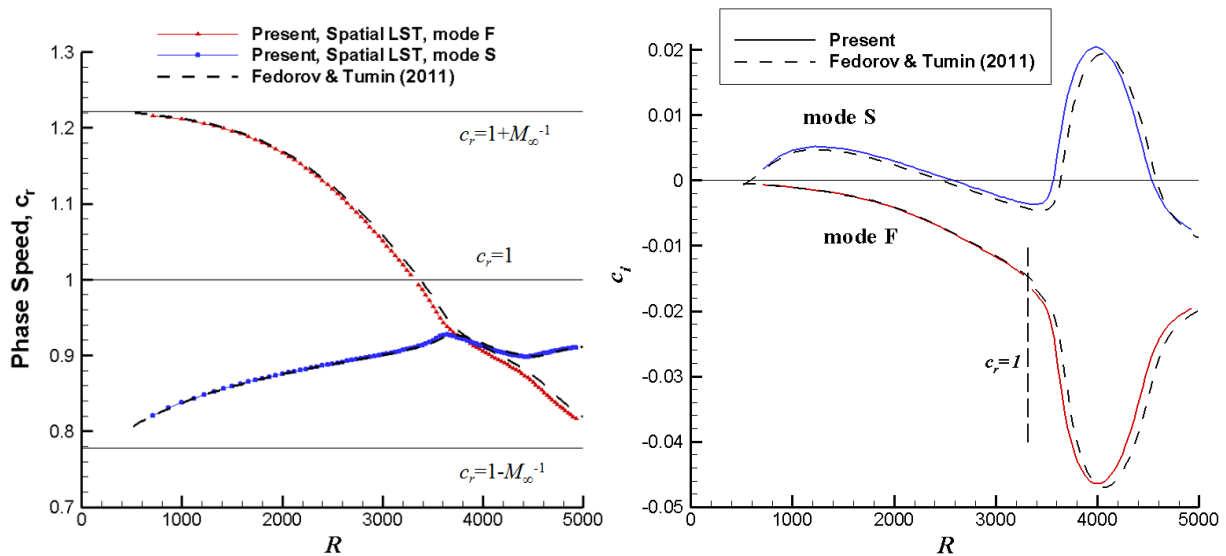


Fig. 3 Plot of (a) real and (b) imaginary part of phase speed of mode F and mode S

Based on the definitions of frequency F and Reynolds number R , non-dimensional angular frequency $\omega (=2\pi f\delta/U_\infty)$ obeys the following relation.

$$\omega = FR \times 10^{-6} \quad (4)$$

According to Eq. (4), the angular frequency for the synchronization point of $F=50$ is found to be $\omega_s \approx 0.1904$ ($R_s \approx 3808$, see Fig. 3a). The phase speed curves with respect

to R of Fig. 4 vary with the frequency F . However, when phase speed is plotted with respect to the angular frequency ω , all the curves are collapsed almost into a single curve as shown in Fig. 4. The same observation was made by Fong et al. (2011). Since angular frequency for synchronization point would also be invariant ($\omega_s=0.1904$), the synchronization point R_s for different frequency F can be simply predicted by $R_s=\omega_s/F \times 10^6$. For example, synchronization points for $F=40$ and 60 will be approximately $R_s \approx 4760$ and 3173, respectively. We also carried out stability analyses for $M_\infty=5.92$ flat plate boundary layer. Freestream conditions are set as $T_\infty=46.69K$ and $p_\infty=742.76Pa$ following Maslov's experiment (Maslov 2001). Fong et al. (2011) also used the same conditions in their DNS study. Results showed good agreement and the angular frequency for synchronization is found to be $\omega_s \approx 0.111$

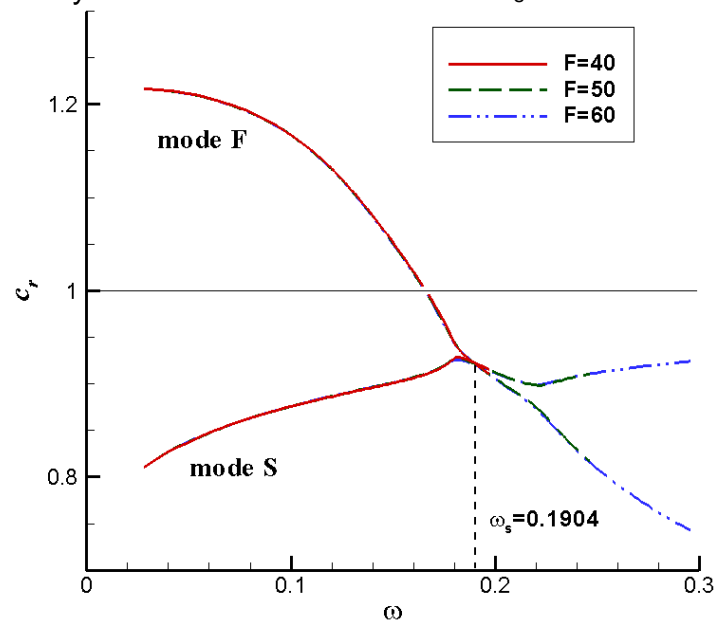


Fig. 4 Plot of real part of phase speed with respect to angular frequency for $F=40, 50,$ and 60

4. MEAN FLOW CALCULATION

The mean flow data for boundary layer over a hump is obtained from the solution of PNS equations. Free-stream conditions are the same with those used in the preceding section ($M_\infty=4.5, T_\infty=61.11K, Re=10^7/m$). Adiabatic wall boundary condition is imposed. We note that general coordinate system is employed for both PNS calculation and PSE analysis of the present study. The x_2 coordinate is in the same direction with that of y coordinate of Cartesian system. The hump center locations are $L=1.0$ m and 1.6 m which correspond to the cases of upstream and downstream of the synchronization point of $F=50$, respectively. We comment here that the synchronization point for $F=50$ was found to be $x=1.45$ m. The hump width and height are fixed at $b=0.1$ m and $h=0.002$ m for both cases. The hump height is approximately 46.3% and 36.6% of local boundary layer thickness (δ_{99}) at $L=1.0$ and 1.6 m, respectively. The streamwise extent of the computational domain is specified such that the inflow and outflow boundaries are at $x=0.4$ m and $x=3.4$ m, respectively. The height of the

computational domain is set to be 800 times the boundary layer length scale at the inflow boundary, i.e. 800δ at $x=0.4$ m ($=0.16$ m). Similarity solution of flat plate boundary layer at the inflow boundary ($x=0.4$ m) is used as inflow condition. 1501 grid points with uniform spacing ($\Delta x=0.002$ m) which ensures 100 grid points over the hump is used in streamwise direction and 501 grid points are distributed in the y -direction with clustering near the surface.

Figure 5 shows skin friction coefficient curves for the above two cases together with that for flat plate case. The vertical dashed line in the figure indicates the streamwise location of synchronization point. We see that the skin friction around the hump is very much deviated from that over a flat plate as expected. The skin friction decreases and rises sharply over a fore part of the hump region. It then decreases around the hump center and increases again to asymptotically reach the value of the flat plate boundary layer. Contrast to subsonic cases, the lowest value of the skin friction appears at an upstream location of the hump center as discussed in our previous study for supersonic boundary layer (Park and Park 2013). This implies that separation would first occur at a location upstream of hump center if the height increases. The reason for this can be easily explained. The flow becomes compressed as the hump center is approached while the flow expands beyond the hump center. This expansion accelerates the flow in the downstream of the hump resulting in the increase of skin friction coefficient. We comment here that the peak deviation of skin friction from that of the flat plate in the downstream region of the hump was smaller in this case than in subsonic flow cases.

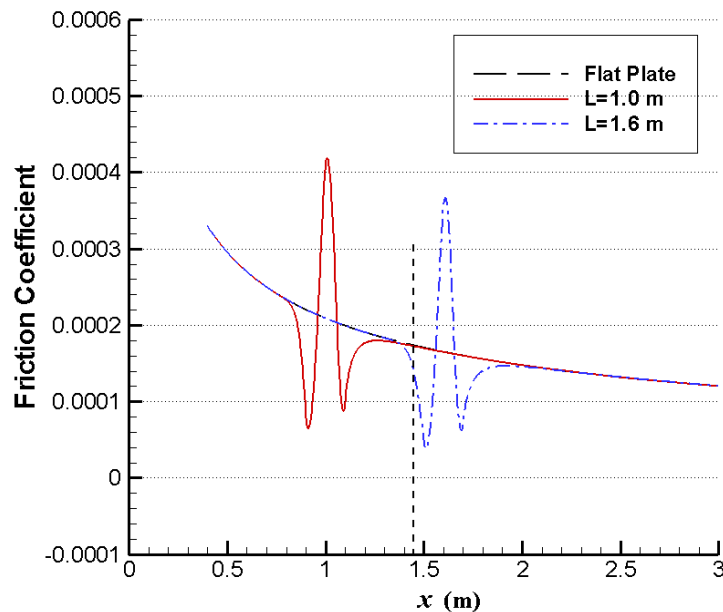


Fig. 5 Skin friction coefficient curves of boundary layer over a hump

5. LINEAR PSE ANALYSIS OF MODE S

5.1 Linear Instability of Mode S

We first perform linear PSE analyses for the evolution of mode S in $M_\infty=4.5$ flat plate boundary layer over a hump. PNS solution is used as mean flow data. For the

region upstream of PNS computational domain, similarity solution of boundary layer equation is taken as mean flow data.

For the stability calculation, the grid distribution in x_2 -direction is chosen differently from that for the mean flow calculation. The mean flow data at stability grid points were obtained by interpolation of those from the PNS calculation. Test calculations were carried out with various grid distributions for stability analysis with the same mean flow data to verify that the interpolation of the mean flow data does not affect the stability results. We chose 201 grid points within 200δ in x_2 -direction with clustering near the solid boundary for stability analysis. Figure 6 contains growth rate curves of $F=50$ for the cases of hump of Fig. 5. Throughout the present study, growth rates (σ) are based on integrated disturbance kinetic energy whose definition can be found in Park and Park (2013). The hump center locations $L=1.0$ m and 1.6 m correspond to $R=3162.3$ and 4000 , respectively. PSE calculation is initiated at $R=774.6$ and the curve for the flat plate case is plotted together in both figures.

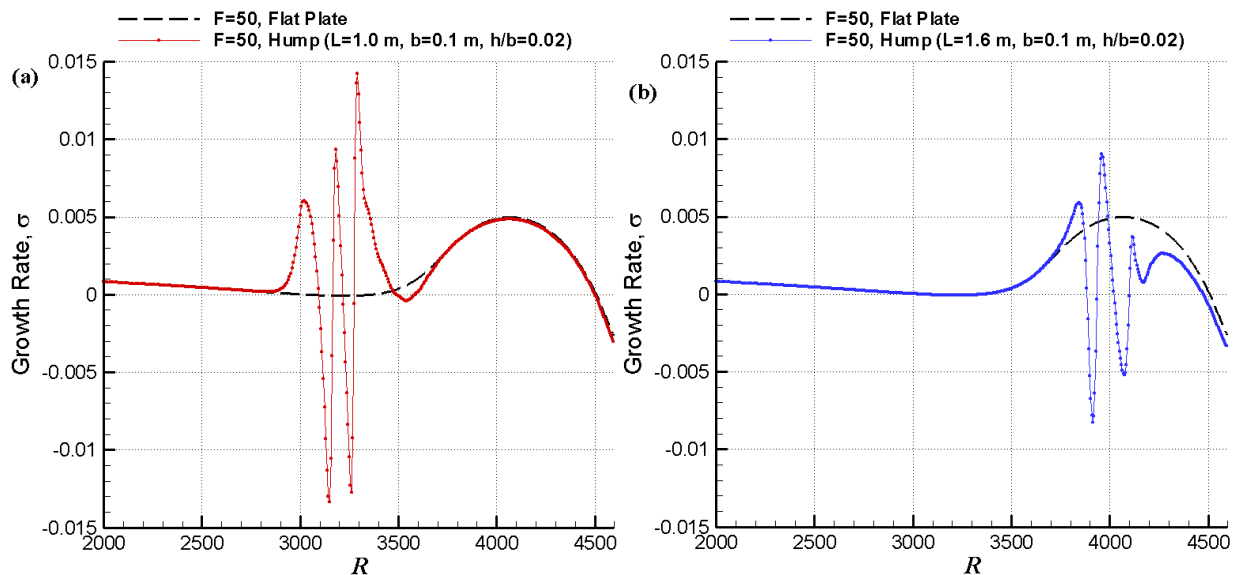


Fig. 6 Growth rate curves of mode S at $F=50$ for hump centered at
 a) $L=1.0$ m and b) $L=1.6$ m

We note here that the mean flow variation in streamwise direction must be small to ensure the reliability of PSE results. Large change of mean flow within one wave length of the instability wave may deteriorate the validity of basic approximation of PSE formulation. To alleviate this issue, we are considering a smooth hump with very low height to width ratio (e.g. $h/b=0.02$) which yields very mild change of mean flow around the hump. This configuration is chosen to justify the use of PSE approach for stability analysis. Moreover, this configuration is also expected to cause only convective instability which is the focus of the present study. We comment here that based on calculated α , the wave length (λ_x) of mode S at $F=50$ is estimated to be around 0.011 m which is approximately 5.5% of the hump width. This implies that variation of mean flow over one wave length around the hump is not likely to be significant.

We see from Fig. 6 that the growth rate over a hump deviates very much, as expected, from that of the flat plate case. The instability wave undergoes sequences of abrupt destabilization and stabilization as it passes the hump. Consequently, the growth rate becomes higher and lower alternatively compared to the flat plate case.

The hump location of $L=1.6$ m is seen to be in the middle of unstable region of large growth rate for flat plate case. For this hump case (Fig. 6b), we see that the growth rate is seen to be smaller than that of the flat plate case over most of the hump region. From this, we can easily expect that the overall effect of the hump would be stabilization of the mode S. To quantitatively evaluate the overall influence of the hump, N -factor which represents logarithmic measure of amplification was computed by integrating the growth rate along streamwise coordinate.

$$N = \int_{x_{1,0}}^{x_1} \sigma(\bar{x}_1) d\bar{x}_1 \quad (4)$$

N -factor curves for both cases of Fig. 6 are plotted in Fig. 7 together with that for the flat plate case. For the case of $L=1.0$ m, we see that N -factor becomes higher than that of flat plate case beyond the hump. This destabilization effect of hump agrees well with the findings from previous studies for first mode instability waves in subsonic and low supersonic Mach number cases (Park and Park 2013). In contrast to this, we note that for the case of $L=1.6$ m, N -factor becomes much smaller compared to that of the flat plate case. This implies that certain combination of frequency and hump location can stabilize convective instability of the mode S in hypersonic boundary layer. We recall that $x=1.0$ m and $x=1.6$ m are upstream and downstream locations of the synchronization point for $F=50$. As already discussed in Fong et al. (2011), present results also indicate that the hump located downstream of synchronization point can stabilize the mode S although the roughness of the present study is a smooth hump with very small height to width ratio. This would be a possible explanation for the observation that roughness can delay hypersonic boundary layer transition under certain conditions. More detailed investigations will be given in the following sections.

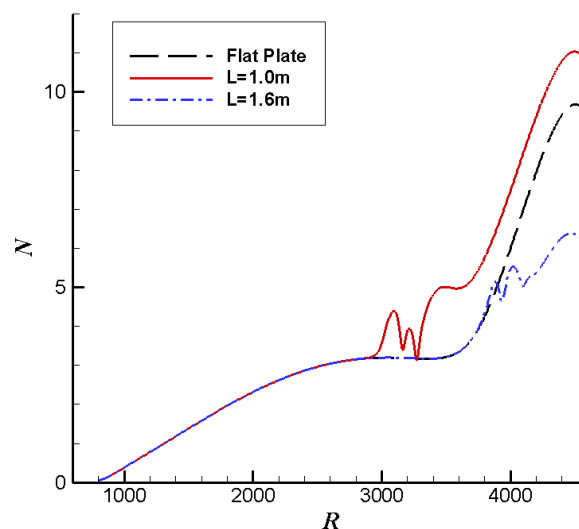


Fig. 7 N -factor curves of mode S at $F=50$

5.2 Effect of Hump Height and Location

To examine the effect of hump location, analyses for humps at several streamwise locations are carried out. Figure 8 shows N -factor curves of $F=50$ with fixed hump geometry ($b=0.1$ m and $h/b=0.02$). Figure 8a corresponds to several hump center locations at upstream of the synchronization point ($x_s \approx 1.45$ m, $R_s \approx 3808$). Vertical dashed lines in the figure denotes the hump center locations. We see from Fig. 8a that humps at far upstream from the synchronization point give a smaller influence ($L=0.8$ m and $L=0.9$ m) on the growth rate. Compared to the flat plate case, the hump at $L=0.8$ m results in slightly smaller N -factor and the hump at $L=0.9$ m shows almost the same amplification with the flat plate case. Ahead of the synchronization point, the hump brings in greater overall destabilization effect as the hump location moves downstream ($L=1.0$ m and $L=1.2$ m). Destabilization becomes greater as the hump gets closer to the synchronization point. On the contrary, we see in Fig. 8b that effect of hump is toward stabilization when the hump center locations are at downstream of the synchronization point. We also see that there is a location where hump the yields the greatest stabilization. For the cases shown in Fig. 8, the hump at $L=1.6$ m exhibits the greatest stabilization and the stabilization effect becomes weaker as the hump moves further downstream.

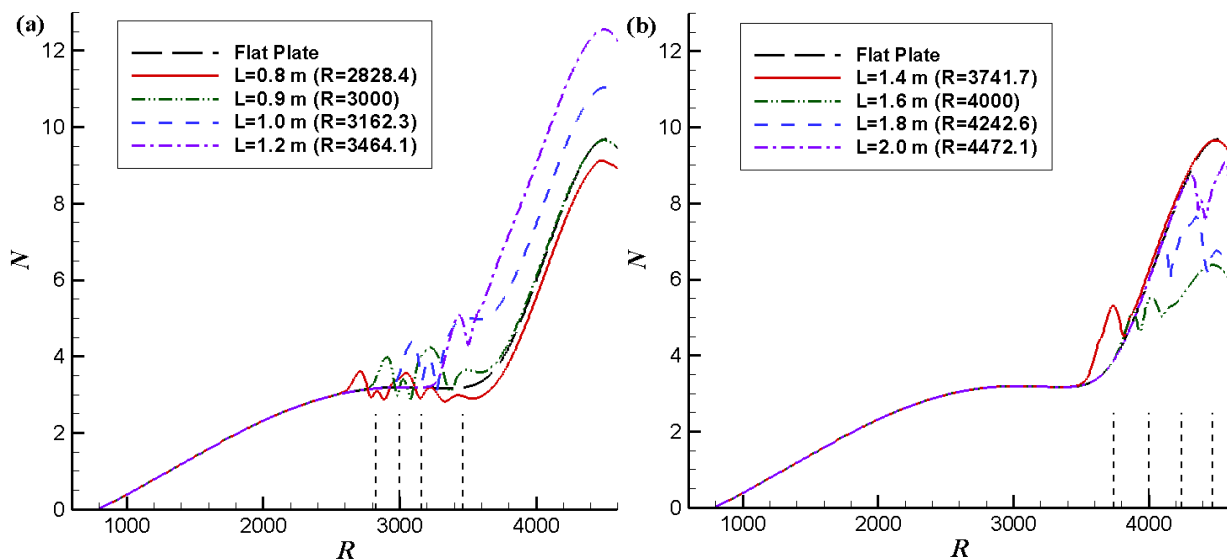


Fig. 8 N -factor curves of mode S for humps at various streamwise locations ($b=0.1$ m, $h/b=0.02$ and $F=50$)

5.3 Overall Influence of Hump on N -Factor Envelope

In the previous subsection, influence of hump height and location on the instability of mode S are examined for a single fixed frequency of $F=50$. To evaluate an overall influence of specific hump, the instability for a wide range of frequency needs to be examined. We carried out linear PSE analyses for various frequencies and resulting N -factor curves are plotted in Fig. 9. The frequency ranges from $F=80$ to $F=40$ with an interval of 2. Figure 9a shows the results for the case of flat plate boundary layer without hump. Results for hump at $L=1.2$, 1.6 , and 2.0 m are plotted in Figs. 9b-9d. Hump half width and height are fixed at $b=0.1$ m and $h/b=0.02$. From the comparison of

Fig. 9a through 9d, we easily see that humps at different locations yield different overall influence.

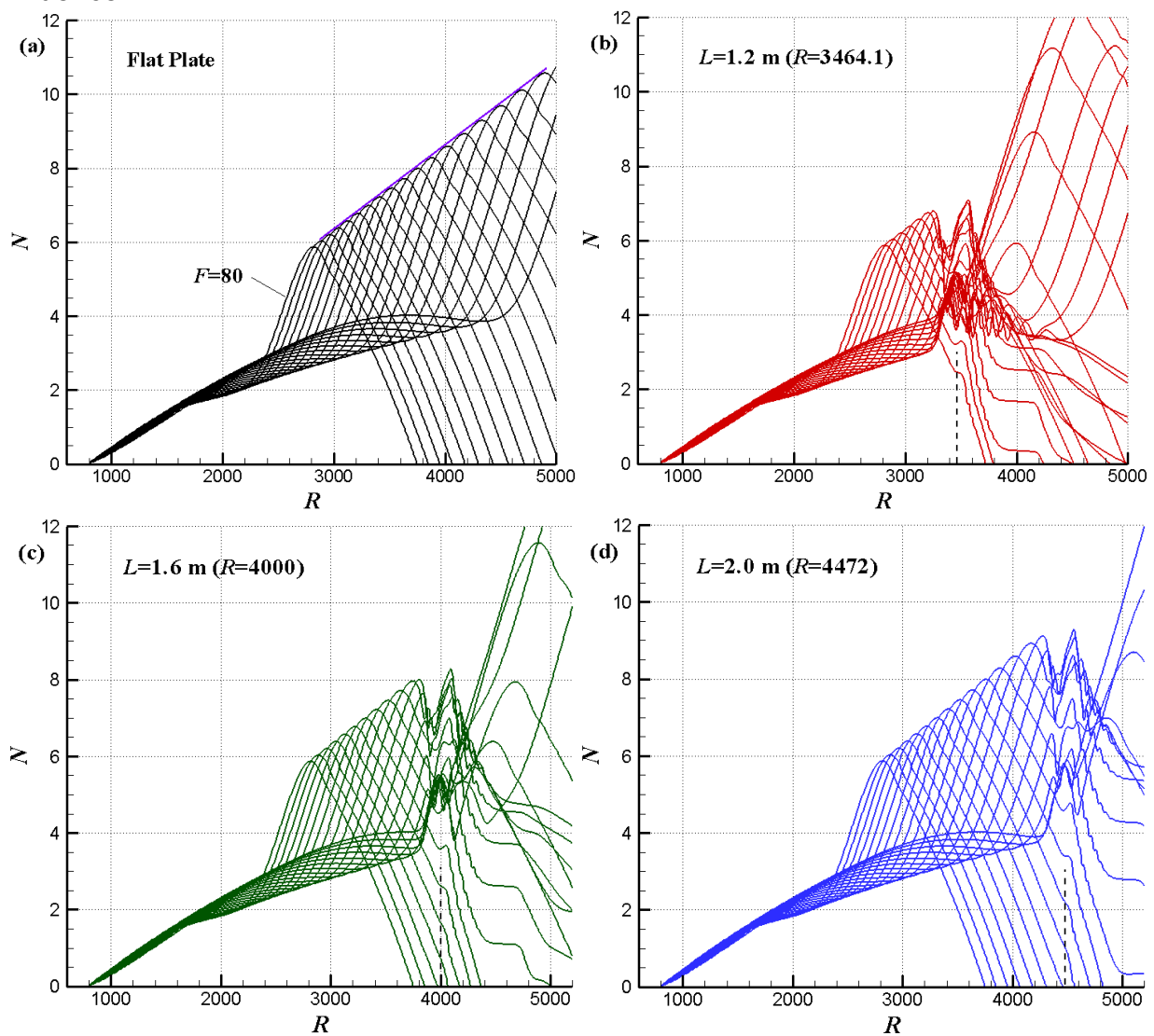


Fig. 9 N -factor curves of mode S for $F=40\sim 80$
 a) flat plate b) hump at $L=1.2$ m c) $L=1.6$ m and d) $L=2.0$ m

When N -factor curves for various frequencies are plotted together (see Fig. 9), N -factor envelop curve can be determined. For example, the straight line drawn in Fig. 9a is an estimation for N -factor envelope curve. Then, we can identify the streamwise position at which N -factor first exceeds certain specified value. If we are interested in the location corresponding to $N=10$, the location is seem to be at $R_{N=10}\approx 4624$ (Fig. 15a) which amounts to $x_{N=10}\approx 2.14$ m. In the same manner, $N=10$ locations for the cases of $L=1.2$, 1.6, and 2.0 m are found to be approximately $x_{N=10}\approx 1.67$, 2.08, and 2.50 m, respectively. In terms of $x_{N=10}$, the hump at $L=1.2$ m has overall destabilization influence and the hump at $L=1.6$ m has almost same influence. On the other hand, the hump at $L=2.0$ seems to yield overall stabilization influence on the boundary layer.

We carried out calculations for more cases and determined the streamwise locations where N -factor first exceeds 10 ($x_{N=10}$). Figure 10 shows the locations of $N=10$ for several hump locations and two different heights ($b=0.1$ m). The symbols of the figure indicate actual computation points. The horizontal solid line in the figure represents $x_{N=10}$ for the case of flat plate. We see that $x_{N=10}$ shifts upstream for the humps located upstream than a specific location. For example, for the humps with $h/b=0.02$, $x_{N=10}$ shifts upstream for the cases where the hump center is ahead of $L=1.6$ m. The upstream shift of $x_{N=10}$ location implies that hump yields overall destabilization effect. As the hump moves downstream, the amount of upstream shift (destabilization effect) decreases. The upstream shift changes to downstream shift (stabilization effect) when the hump location moves downstream beyond a certain position. For example, it is seen that the change occurs between $L=1.6$ and $L=1.7$ m for the hump with $h/b=0.02$. Beyond this point, downstream shift becomes greater with more downstream position of the hump. However, at further downstream location, we see that $x_{N=10}$ returns back to that of flat plate case. We see from the figure that the hump located beyond $L=2.4$ m does not affect the location of $x_{N=10}$. This is due to the fact that the mean flow data is the same with those of flat plate up to $N=10$ location for the case of far downstream hump. It can be inferred from Fig. 10 that the two-dimensional smooth hump within a certain range of streamwise location can yield overall stabilization effect on the linear evolution of mode S.

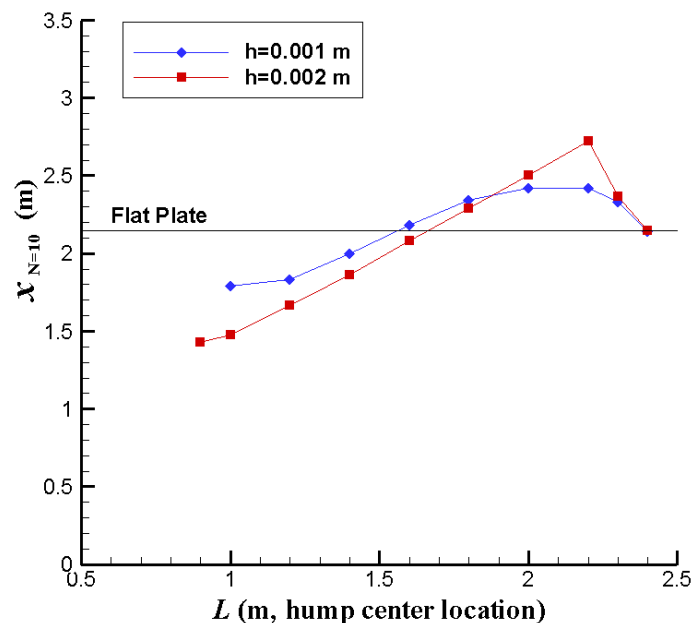


Fig. 10 The locations at which N -factor first exceeds 10

5.4 Mach 5.92 Boundary Layer

We performed additional calculations for $M_\infty=5.92$ boundary layer to verify that stabilization effect is also observed at this Mach number. The mean flow data are obtained from PNS solution in the same manner as in the previous analyses. As mentioned already, free-stream conditions are set as $T_\infty=48.69$ K and $p_\infty=742.76$ Pa which yields the unit Reynolds number of 1.416×10^7 . Fong et al. (2011) studied the

boundary layer at the same free-stream condition by using DNS. They calculated for mode S at $f=100$ kHz over an elliptic roughness at several locations and heights. Their results showed that the mode S was destabilized by the roughness at $x=0.185$ m with height greater than 50% of local boundary layer thickness. On the other hand, the mode S was stabilized by the roughness at $x=0.410$ m with height up to 62.5% of local boundary layer thickness (see Figs. 16b and 16d in Fong et al. 2011).

Based on the free-stream condition, the non-dimensional frequency of $f=100$ kHz is $F \approx 53.6$ and we carried out PSE analysis for the same frequency. Figure 11a shows N -factor curve with respect to x for a hump at $L=0.2$ m with $b=0.05$ m and $h/b=0.03$. The hump height is approximately 62.7 % of the local boundary layer thickness. Initial condition for PSE analysis is imposed at $x=0.04$ m. Figure 11b shows the results for the hump at $L=0.45$ and 0.5 m with $b=0.1$ m and $h/b=0.02$. The hump heights are approximately 55.7 and 52.9 % of the local boundary layer thickness at $x=0.45$ and 0.5 m, respectively. PSE calculation is initiated at $x=0.1$ m. We clearly see from Fig. 11 that the mode S is destabilized by the hump at $L=0.2$ m and stabilized by hump at $L=0.45$ and 0.5 m. This observation qualitatively agrees well with the DNS results of Fong et al. (2011). It has to be noted, however, that the geometry of the roughness is different each other. Despite the difference of the roughness geometry, the basic stabilization mechanism due to roughness element seems to agree each other in both studies.

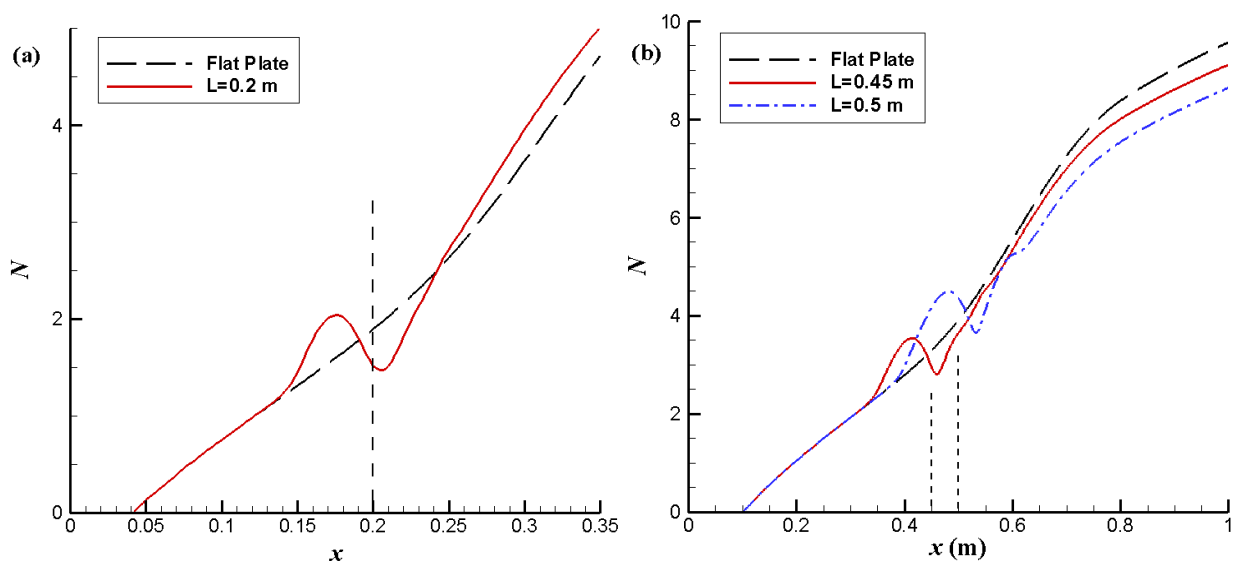


Fig. 11 N -factor curve of mode S at $f=100$ kHz for a) $L=0.2$ m and b) $L=0.45$ and 0.5 m

As already determined by LST analysis (Sec. 3), the angular frequency of the synchronization point was $\omega_s \approx 0.111$. From Eq. (4), the synchronization point for $F \approx 53.6$ is estimated as $R_s \approx 2070.9$ ($x_s = 0.294$ m). This location is in the downstream of $L=0.2$ m and the upstream of $L=0.45$ and 0.5 m. Clearly, stabilization effect occurs for the hump located at downstream of this synchronization point. This is consistent with the observations made in the preceding Mach 4.5 boundary layer case.

To ensure this point, we carried out additional calculations for different frequencies. Figure 12a shows the N -factor curve of $F=40$ for the hump at $L=0.4$ and 0.6 m ($R \approx 2380$ and 2914.8) together with that of flat plate case. Initial condition for PSE

analysis is imposed at $R \approx 752.6$. The synchronization point for $F=40$ is $R_s \approx 2775$ and is noted with arrow in the figure. As shown in Fig. 12a, the synchronization point is between the two hump centers which are marked with vertical dashed lines. Figure 12b shows similar calculations for $F=30$ with humps at $L=0.8$ m ($R \approx 3365.7$) and 1.2 m ($R \approx 4122.1$). The synchronization point for $F=30$ is $R_s \approx 3700$. We also see from Fig. 12b that the mode S is stabilized by the hump located at the downstream of the synchronization point. From the results shown, the stabilization influence of hump whose location is at downstream of the synchronization point can be regarded as a general feature of hypersonic boundary layer.

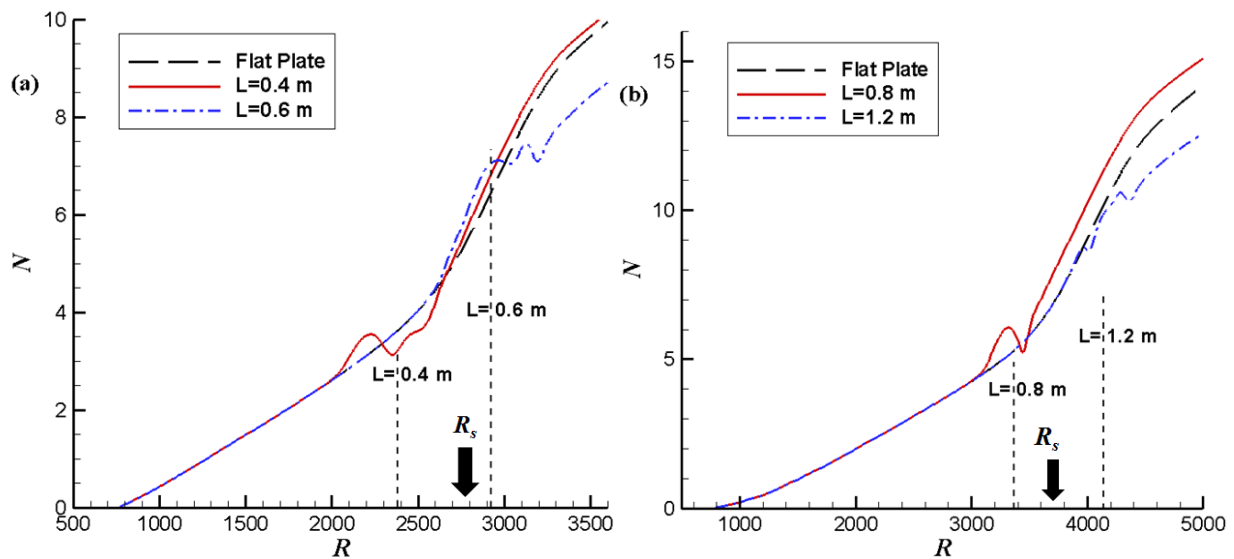


Fig. 12 N -factor curve of a) $F=40$ and b) $F=30$ for $M_\infty=5.92$ boundary layer

6. CONCLUSIONS

In the present study, the influence of hump on the instability of mode S in hypersonic boundary layer was investigated by using PSE analyses. The flat plate boundary layer of $M_\infty=4.5$ and 5.92 were considered. A two-dimensional smooth hump was chosen as roughness geometry. Humps with height smaller than local boundary layer thickness and very small height to width ratio less than 0.03 was considered to ensure very mild change of mean flow around the hump.

The spatial linear stability analysis was carried out for flat plate to identify the synchronization point. The linear PSE analyses were carried out for linear evolution of mode S in $M_\infty=4.5$ boundary layer with hump located at upstream and downstream of the synchronization point. The mean flow for PSE analysis was obtained from PNS solution. The results showed that the mode S is destabilized by the hump when it is located at upstream of the synchronization point. The destabilization effect due to hump is consistent with the observations for subsonic and supersonic boundary layers of previous studies. On the other hand, the stabilization influence was identified for the hump when it is located at downstream of the synchronization point. It is consistent with the DNS results of recent studies with different roughness geometry. Parametric

studies were carried out to examine the effect of hump location and height. The results for several hump locations confirmed that the hump located at a downstream position of synchronization point stabilizes mode S. Results for different hump heights revealed that both destabilization and stabilization effect was enhanced as the hump height increases. Analyses for various frequencies were carried out to examine the overall effect of hump. For the hump at several streamwise locations, the location at which N -factor first exceeds value of 10 was identified from all N -factor curves envelope. The results showed that the hump within specific region pushes $N=10$ location downstream compared to the case of flat plate. The analyses for $M_\infty=5.92$ were also carried out and the same stabilization influence of hump was identified.

REFERENCES

- Holloway, P. F. and Sterrett, J. R. (1964), "Effect of Controlled Surface Roughness on Boundary-Layer Transition and Heat Transfer at Mach Numbers of 4.8 and 6.0," NASA TN D-2054.
- Fujii, K. (2006), "Experiment of the Two Dimensional Roughness Effect on Hypersonic Boundary-Layer Transition," *Journal of Spacecraft and Rockets*, **43**(4), 731-738.
- Fedorov, A. and Tumin, A. (2011), "High-Speed Boundary-Layer Instability: Old Terminology and a New Framework," *AIAA Journal*, **49**(8), 647-1657.
- Duan, L., Wang, X., and Zhong, X. (2009), "A High-Order Cut-Cell Method for Numerical Simulation of Hypersonic-Boundary Transition with Arbitrary Surface Roughness," AIAA 2009-1337.
- Duan, L., Wang, X., and Zhong, X. (2010), "A High-Order Cut-Cell Method for Numerical Simulation of Hypersonic-Boundary Layer Instability with Surface Roughness," *Journal of Computational Physics*, **229**(19), 7207-7237.
- Fong, K. D., Wang, X., and Zhong, X. (2011), "Numerical Simulation of Roughness Effect on the Stability of a Hypersonic Boundary Layer," Seventh International Conference on Computational Fluid Dynamics (ICCFD7), ICCFD7-1502, Hawaii.
- Nayfeh, A. H., Ragab, S.A., and Al-Maaitah, A. A. (1988), "Effect of Bulges on the Stability of Boundary Layers," *Phys. Fluids*, **31**(4), 796-806.
- Masad, J. A. and Iyer, V. (1994), "Transition prediction and control in subsonic flow over a hump," *Phys. Fluids A*, **6**(1), 313-327.
- Park, D. and Park S. O (2013), "Linear and Non-linear Stability Analysis of Incompressible Boundary Layer over a Hump," *Computers and Fluids*, **73**, 80-96.
- Park, D. and Park S. O (2013), "Influence of Two-Dimensional Smooth Humps on Linear and Non-Linear Instability of a Supersonic Boundary Layer," *Computers and Fluids*, **79**,140-149.
- Tannehill, J. C., Miller, J. H., and Lawrence, S. L. (1999), "Development of an Iterative PNS Code for Separated Flows," AIAA-99-3361.
- Tannehill, J. C., Miller, J. H., and Lawrence, S. L. (2000), "Iterative PNS Algorithms for Solving 3-D Supersonic Flows with Upstream Influences," AIAA 2000-0821.
- Hejranfar, K., Esfahanian, V., and Darian, H. M. (2007), "On the Use of High-Order Accurate Solution of PNS Schemes as Basic Flows for Stability Analysis of Hypersonic Axisymmetric Flows," *ASME Transactions*, **129**, 1328-1338.

- Herbert, T. (1997), "Parabolized Stability Equations," *Annu. Rev. Fluid. Mech.*, **29**, 245-283.
- Chang, C.-L., Malik, M. R., Erlebacher, G., and Hussaini, M. Y. (1993), "Linear and Nonlinear PSE for Compressible Boundary Layers," NASA CR-191537, ICASE Report No.93-70.
- Chang, C.-L. (2004), "Langley Stability and Transition Analysis Code(LASTRAC) Version 1.2 User Manual," NASA TM-2004-213233.
- Iyer, V. (1990), "Computation of Three-Dimensional Compressible Boundary Layers to Fourth-Order Accuracy on Wings and Fuselages," NASA CR-4269.
- Malik, M. R. (1990), "Numerical Methods for Hypersonic Boundary Layer Stability," *Journal of Computational Physics*, **86**, 376-413.
- Fedorov, A. V., and Khokhlov, A. P. (2001), "Prehistory of Instability in Hypersonic Boundary Layer," *Theoretical and Computational Fluid Dynamics*, **14**, 359-375.
- Maslov, A. A., Shpiyuk, A. N., Sidorenko, A. A., Arnal, D. (2001), "Leading-edge Receptivity of a Hypersonic Boundary Layer on a Flat Plate," *Journal of Fluid Mechanics*, **426**, 73-94.